Cell, Vol. 93, 1241–1252, June 26, 1998, Copyright ©1998 by Cell Press

A Critical Role for Amino-Terminal Glutamine/Asparagine Repeats in the Formation and Propagation of a Yeast Prion

Angela H. DePace,*§ Alex Santoso,*§
Paul Hillner,*† and Jonathan S. Weissman*‡
*Department of Cellular and Molecular Pharmacology
†Howard Hughes Medical Institute
University of California–San Francisco
San Francisco, California 94143-0450

Summary

The yeast [*PSI*$^+$] factor propagates by a prion-like mechanism involving self-replicating Sup35p amyloids. We identified multiple Sup35p mutants that either are poorly recruited into, or cause curing of, wildtype amyloids in vivo. In vitro, these mutants showed markedly decreased rates of amyloid formation, strongly supporting the protein-only prion hypothesis. Kinetic analysis suggests that the prion state replicates by accelerating slow conformational changes rather than by providing stable nuclei. Strikingly, our mutations map exclusively within a short glutamine/asparagine-rich region of Sup35p, and all but one occur at polar residues. Even after replacement of this region with polyglutamine, Sup35p retains its ability to form amyloids. These and other considerations suggest similarities between the prion-like propagation of [*PSI*$^+$] and polyglutamine-mediated pathogenesis of several neurodegenerative diseases.

Introduction

Virtually all denatured proteins have a strong propensity to form amorphous aggregates. This aggregation is largely driven by the association of hydrophobic regions that are normally buried in the native structure (for review, see Jaenicke and Seckler, 1997). In contrast to these more frequent disordered aggregates, some proteins form ordered aggregates called amyloid fibrils. Amyloidogenic proteins show no obvious sequence similarity, nor do their native folds resemble one another. Yet despite this diversity amyloid fibrils appear to share a similar architecture.

Amyloid fibrils are cross β-sheet structures in which the individual β strands run perpendicular to the long axis of the fibril, whereas the faces of the β sheets extend parallel to it (Lansbury et al., 1995; Sunde and Blake, 1997). These fibrils are roughly 100 Å in diameter and are typically composed of 4–6 interwoven protofilaments. Recent X-ray diffraction studies suggest that the β sheets composing the individual protofilaments are twisted, resulting in a helical conformation propagating along the amyloid axis (Sunde et al., 1997; see, however, Lazo and Downing, 1998). The ordered structure of amyloids allows them to bind the dye Congo red at regular intervals, leading to a characteristic red-green birefringence under polarized light. Despite these shared structural features, electron microscopy (EM) and atomic force microscopy (AFM) (Harper et al., 1997a) analyses indicate that there are ultrastructural variations (e.g., differences in the number and packing of the protofilaments) between the amyloids. It is also possible that individual protein monomers retain partial native structure within the amyloid (Liu et al., 1998).

To date, ~20 proteins have been found to form amyloids associated with human disease. These include the mammalian prion protein, PrP, the infectious protein implicated as the causative agent of transmissible spongiform encephalopathies (see Caughey and Chesebro, 1997; Prusiner et al, 1998). PrP forms amyloid fibrils that, at least under some conditions, are associated with the infectious agent. Similarly, some non-prion neurodegenerative diseases, such as Alzheimer's and Huntington's disease, also involve amyloid formation. In Huntington's, as well as several other neurodegenerative diseases, amyloid formation appears to be caused by expansion of a polyglutamine (polyGln) tract (e.g., Paulson et al., 1997; Scherzinger et al., 1997). Finally, systemic amyloidoses result from the aggregation of a number of proteins such as lysozyme and transthyretin (TTR) (Wetzel, 1997).

Despite active research, many basic questions about the conversion from native state to amyloid fibril remain unanswered. For example, little is known about what stabilizes amyloid structures. In particular, how sensitive is amyloid formation to changes in primary sequence? Are amyloids, like amorphous aggregates, principally stabilized by hydrophobic interactions? The mechanism of propagation of infectious prion diseases and its relationship to that of noninfectious amyloidoses is also poorly understood (Harper and Lansbury, 1997; Prusiner et al., 1998). For example, what is the nature of the rate-limiting step in de novo formation of amyloids, and how do preformed fibrils accelerate this process? Lastly, our understanding of the role of cellular factors, such as molecular chaperones, in promoting formation of amyloids is incomplete (Chernoff et al., 1995; Kaneko et al., 1997). In particular, do in vitro conversion reactions using purified proteins accurately reproduce the propagation of disease or infection in vivo?

The prion-like phenomenon [*PSI*$^+$] of the yeast *Saccharomyces cerevisiae* provides a powerful model system to address these questions. [*PSI*$^+$] is a non-Mendelian trait that causes suppression of nonsense mutations (Cox et al., 1988). This nonsense suppression is thought to result from the conversion of the translation termination factor Sup35p from a soluble and functional state into insoluble and inactive amyloid fibrils (Wickner et al., 1995; see Lindquist, 1997). [*PSI*$^+$] appears to propagate by a prion-like mechanism in which the amyloid form of Sup35p promotes the conversion of newly made soluble Sup35p to insoluble fibrils. The increased nonsense suppression caused by the [*PSI*$^+$] factor can be readily monitored by using a strain carrying a marker gene with a nonsense mutation. Thus, the [*PSI*$^+$] phenomenon allows

‡To whom correspondence should be addressed.
§These authors contributed equally to this work.

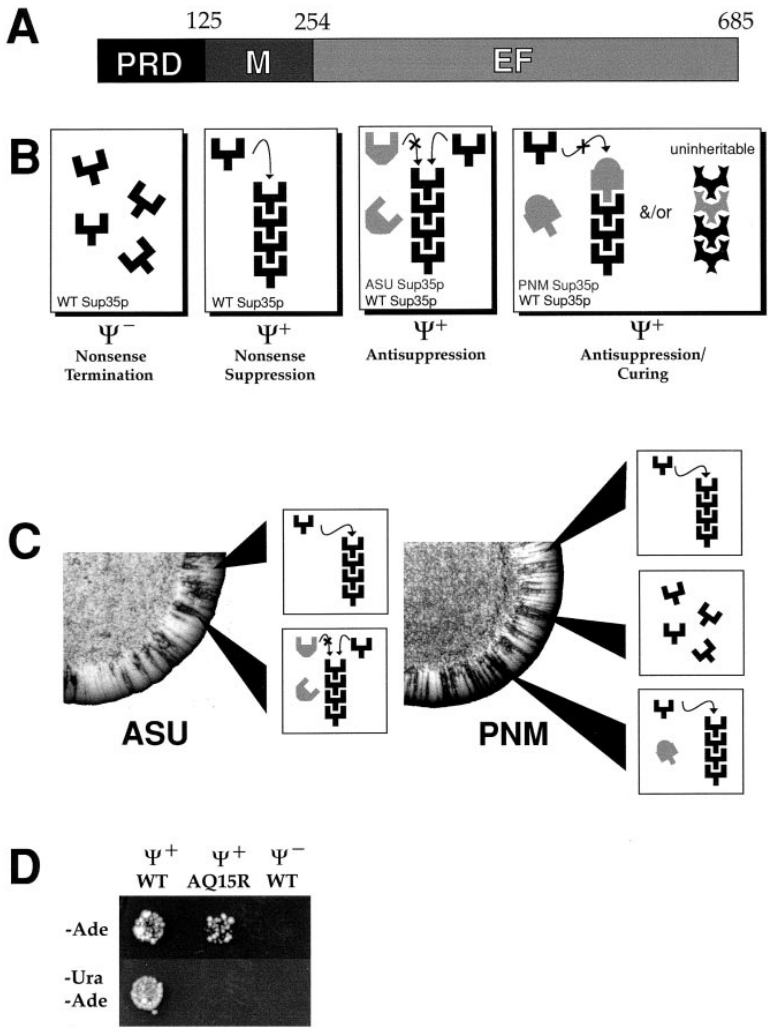

Figure 1. Illustration of the Screen for ASU and PNM Mutants

(A) Schematic of Sup35p domain structure. Residue numbers are indicated on the top of the schematic.

(B) Illustration of the logic underlying the screen for ASU and PNM mutants. Throughout the figures, strain background is indicated by ψ^+ for [*PSI*$^+$] and by ψ^- for [*psi*$^-$]. The Sup35p alleles present are indicated in the lower left of each panel and diagramatically with solid and gray shapes representing WT Sup35p and mutant Sup35p, respectively. The phenotypes resulting from expression of the indicated Sup35p alleles are listed in the bottom row beneath each panel. Amyloids are denoted by stacked monomers, and soluble Sup35p are denoted by unattached subunits. Two hypothetical mechanisms for PNM mediated curing are illustrated in the final panel. These involve either capping of amyloids to prevent further monomer addition (left) or conformational change, which renders the amyloids uninheritable (right).

(C) Examples of sectored colonies resulting from expression of ASU and PNM mutants. The solubilization states of the various alleles of Sup35p that could lead to the observed color changes are illustrated on the right of the colony (see text). Diagrams and symbols are as in (B).

(D) Sample data demonstrating plasmid-dependent antisuppresion. Growth of a [*PSI*$^+$] strain initially bearing AQ15R on a URA3 marked plasmid on the indicated medium is shown. [*PSI*$^+$] and [*psi*$^-$] expressing WT protein are shown for comparison.

one to assess the microscopic aggregation state of the Sup35p protein in vivo by examining the macroscopic properties of a yeast colony.

Here, we use the [*PSI*$^+$] system to define the sequence requirements for efficient formation and prion-like propagation of Sup35p amyloids in vivo. In addition, using an in vitro conversion reaction (Glover et al., 1997; King et al., 1997; Paushkin et al., 1997), we have exploited mutant Sup35p proteins that are defective in amyloid formation to help elucidate the mechanism of prion propagation.

Results

Mutagenesis of the Sup35p Reveals a Requirement for Glutamine/Asparagine-Rich Sequences

Sup35p is composed of three domains (Ter-Avanesyan et al., 1993) (Figure 1A). The N-terminal prion determining domain (PrD) is necessary and sufficient for propagation of aggregates. Deletion of this domain allows Sup35p to remain soluble even in [*PSI*$^+$] cells (Paushkin et al., 1996). Conversely, fusion of the PrD to GFP confers aggregation of the fusion protein in a [*PSI*$^+$]-dependent manner (Patino et al., 1996). The middle domain (M) of Sup35p is a highly charged region of unknown function. The C-terminal domain, referred to as EF because of its homology to elongation factors, encodes a translation termination activity (Stansfield et al., 1995). Expression of this domain without a PrD provides a pool of soluble, active EF domain, resulting in a loss of nonsense suppression even in cells containing wild-type (WT) Sup35p aggregates (Ter-Avanesyan et al., 1993). Hereafter, [*PSI*$^+$] refers to the presence of heritable aggregates; [*PSI*$^+$] yeast that also contain soluble EF, and therefore no longer exhibit nonsense suppression, will be referred to as antisuppressed.

We have developed a genetic screen to identify PrD mutants that are defective in amyloid formation and propagation. This screen is based on the fact that such mutants will remain soluble even in a [*PSI*$^+$] yeast cell that contains WT Sup35p aggregates, thereby conferring an antisuppressor (ASU) phenotype (Figure 1B). To track the suppression phenotype, a [*PSI*$^+$] strain harboring a nonsense mutation in the *ADE1* gene was used (Chernoff et al., 1995). In yeast retaining their nonsense suppression phenotype, functional Ade1p is produced resulting in white colonies on complete medium (YPD) and an ability to grow on medium lacking adenine (SD-ADE). However, in either [*psi*$^-$] or antisuppressed yeast, Ade1p is truncated and nonfunctional, resulting in red

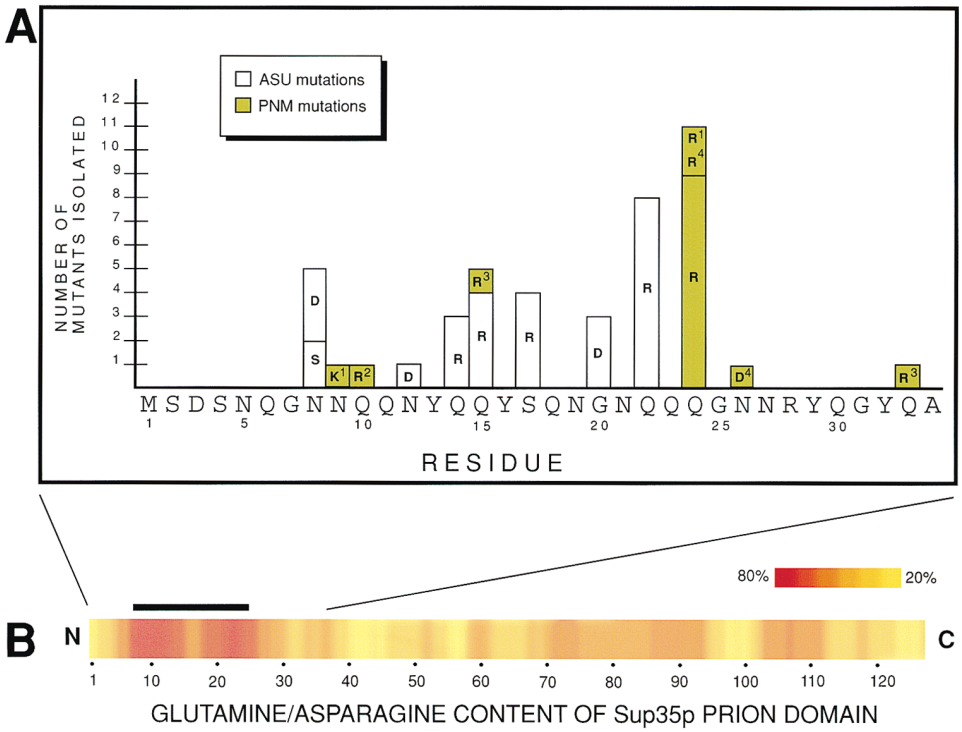

Figure 2. Summary of ASU and PNM Mutants

(A) Bar graph of the frequency and phenotype of the PrD mutants as a function of residue position. Amino acid changes from the WT sequence (x axis) are indicated within the bars. All mutants contain changes within residues 8–24 of the PrD. Double mutants are indicated by a superscript and contain the following changes: (1) PN9K, Q24R; (2) PQ10R, Q91L; (3) PQ15R, Q33R; (4) PQ24R, N26D, where the mutant is denoted by the first letter of the phenotype (A or P) followed by the amino acid changes. For double mutants, changes outside of residues 8–24 are not reported when they do not affect the phenotype.

(B) Average glutamine/asparagine content of the PrD as function of residue number. The color indicates the percent of glutamine and asparagine residues in a window spanning nine amino acids (scale is indicated on the right). The black bar above the graph marks the location of the isolated PrD mutations.

colonies on YPD and failure to grow on SD-ADE. The PrD was uniformly mutagenized using PCR under conditions that favored single nucleotide changes. A library of *sup35* genes with mutagenized PrDs was episomally expressed on a URA3-marked plasmid in a strain that contains chromosomally encoded WT Sup35p.

Yeast expressing compromised PrDs were readily identified because they formed red/white sectored colonies on YPD (Figure 1C). White sectors result from yeast that have lost the plasmid expressing mutant Sup35p but have retained WT aggregates. Conversely, red sectors result from either an ASU phenotype caused by the presence of the mutant Sup35p or conversion to [*psi*$^-$] (i.e., permanent loss of all Sup35p aggregates). The ASU phenotype was confirmed by the lack of functional Ade1p under growth conditions that require retention of the mutant Sup35p plasmid (i.e., inability to grow on SD-ADE, -URA, Figure 1D). In contrast, the nonsense suppression phenotype returned following plasmid loss (i.e., growth on SD-ADE medium). The ASU mutants were then examined for their ability to cause permanent conversion to a [*psi*$^-$] state. Such "curing" alleles are referred to as Psi No More (PNM) mutants (Doel et al., 1994). Cured yeast were identified by the presence of red colonies on 5-FOA medium, which selects for yeast that have lost the plasmid expressing the mutant Sup35p. The fraction of cured cells caused by transient expression of PNM mutants ranged from ~1%–50% and generally increased with expression time. We screened ~15,000 colonies for ASU phenotypes and ~30,000 colonies for PNM phenotypes. In this pool, we estimate that every point mutant is represented 5- to 10-fold. In total, 28 ASU and 13 PNM mutants were sequenced. The observed redundancy in recovered alleles is in good agreement with this estimated overrepresentation (Figure 2A). The individual mutations are denoted by the first letter of the phenotype (A or P) followed by the amino acid changes.

Unexpectedly, all ASU and PNM mutants contained changes in a short region at the extreme N terminus of the PrD between residues 8 and 24 (Figure 2A). The failure to identify mutations outside of this region was not due to lack of diversity in the original mutant pool, as a number of mutations that did not cause the ASU phenotype were found throughout the PrD. Nor was it because the residues outside this region were unnecessary for PrD function: deletion of residues 53–124 of the PrD resulted in an ASU phenotype (data not shown), and a previously described chromosomal PNM mutant maps outside this region (Doel et al., 1994). Rather, it appears that point mutations outside this region did not result in a sufficiently robust ASU phenotype to pass our screens. Although the entire PrD has a high Gln/Asn content, the subdomain identified by our mutagenesis

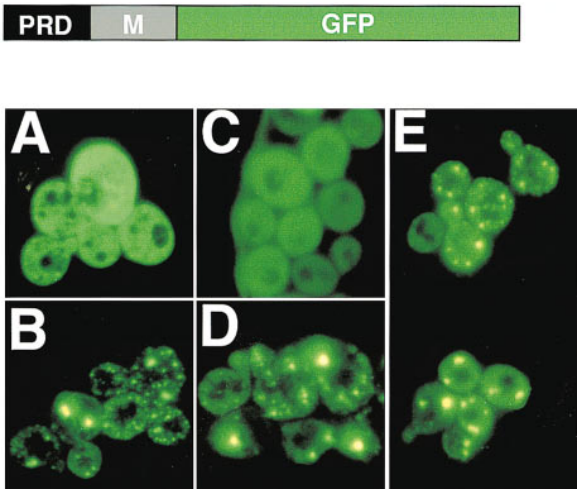

Figure 3. Aggregation State of Mutant PrD as Assayed by GFP Fluorescence

Yeast expressing a PrD-GFP fusion construct were examined 2 hr postinduction. Diffuse fluorescence throughout the cytoplasm is indicative of soluble protein, while bright discrete foci are indicative of protein associated with prion-like Sup35p aggregates. Larger aggregates result in a halo of fluorescence, which is not interpreted as soluble protein. The PSI state and PrD allele are indicated below.
(A) [*psi*$^-$] yeast expressing WT-PrD-GFP.
(B) [*PSI*$^+$] yeast expressing WT-PrD-GFP.
(C) A representative field in which an ASU mutant appears entirely soluble in presence of WT aggregates ([*PSI*$^+$] expressing AG20R-PrD-GFP).
(D) A representative field in which an ASU mutant appears to associate predominantly with WT aggregates ([*PSI*$^+$] expressing AQ22R-PrD-GFP).
(E) Representative fields in which ASU mutants appear to partition between soluble pools and discrete foci ([*PSI*$^+$] yeast expressing AQ15R-PrD-GFP [top] and AN8D-PrD-GFP [bottom]).

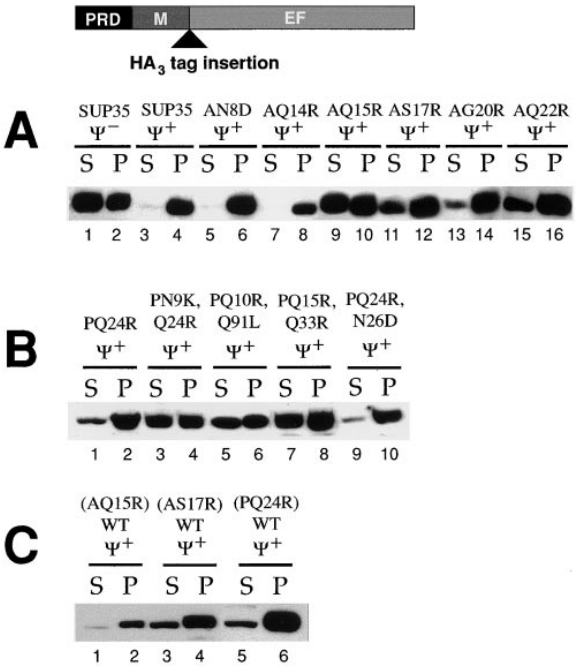

Figure 4. Aggregation State of Mutant PrD Alleles as Assayed by High Speed Centrifugation

Mid–log phase cell extracts were prepared from yeast strains carrying a plasmid expressing the indicated allele of Sup35p. Extracts were centrifuged at 100,000 g, and soluble (S) or pelleted (P) fractions were assayed by Western blot. Plasmid-derived protein was distinguished from WT chromosomal Sup35p by the addition of a hemaglutanin (HA_3) tag between the M and EF domains (schematic at top). The PSI state of the cells and the expressed mutant protein allele are indicated above each set of lanes.
(A) Solubility of WT Sup35p compared to ASU mutant proteins in [*PSI*$^+$] yeast. For comparison, WT Sup35p in [*psi*$^-$] yeast is also shown. Note that the presence of Sup35p in [*psi*$^-$] pellet is not likely to represent prion-like Sup35p aggregates, and thus the levels of soluble protein are an underestimate of the amount of functional Sup35p.
(B) Solubility of PNM mutants in [*PSI*$^+$] yeast.
(C) Solubility of WT Sup35p in [*PSI*$^+$] yeast coexpressing mutant PrD alleles. WT Sup35p was tagged with (HA_3), while mutant protein was untagged and therefore not recognized by Western blot. The untagged mutant protein present is indicated in parentheses above each set of lanes.

shows a particularly strong enrichment for these amino acids (Figure 2B). Moreover, all of the mutations occurred in Gln or Asn residues with the exception of a single Gly and a single Ser mutant. Virtually all mutations resulted in a change to charged amino acids. Particularly striking is the predominance of Gln or Ser to Arg mutations. This is physically reasonable because the bulky and charged Arg side chain is likely to be particularly disruptive to protein–protein interactions. Gly or Asn to Arg mutations are not observed, however, because they would require two nucleotide changes.

ASU and PNM Mutants Show Diminished Ability to Be Recruited into WT Sup35p Aggregates In Vivo

The screen for ASU and PNM mutants was based on the hypothesis that the antisuppression phenotypes resulted from a decreased ability of mutant PrDs to be recruited into WT Sup35p aggregates. We tested this using a GFP-based assay described by Lindquist and coworkers (Patino et al., 1996). WT PrD-GFP converts from a diffuse fluorescence pattern in [*psi*$^-$] cells (Figure 3A) to a punctate pattern in [*PSI*$^+$] (Figure 3B), making it possible to monitor the aggregation state of PrD fusion protein in vivo. Each of the ASU and PNM mutants was fused to GFP and put under control of the inducible CUP1 promoter. Use of an inducible promoter minimizes secondary effects that prolonged expression of mutants might have on the solubility of the WT Sup35p. In contrast to WT PrD-GFP, which had uniformly punctate patterns in [*PSI*$^+$] cells, each mutant led to a mixed population of fluorescent patterns: in individual cells, the fusion proteins either appeared entirely soluble (Figure 3C), in discrete foci (Figure 3D), or more commonly in both (Figure 3E).

We next examined the aggregation state of the mutant PrDs using a centrifugation assay that made it possible to determine the solubility of full-length Sup35p protein expressed from its natural promoter (Patino et al., 1996; Paushkin et al., 1996). In [*PSI*$^+$] cells, Sup35p is in aggregates that are efficiently separated from soluble protein fractions by centrifugation. In contrast, Sup35p in [*psi*$^-$] cells remains predominately soluble following centrifugation (Figure 4A, lanes 1–4). To distinguish mutant

Sup35p from chromosomally encoded WT protein, the mutant proteins were tagged with the HA antigen. Following centrifugation, levels of soluble and aggregated proteins were examined by Western blot analysis. We found that 9 of the 11 ASU and PNM mutants showed significant increases in soluble protein in [*PSI*$^+$] cells (Figures 4A and 4B). As might be expected from its comparatively weak ASU phenotype, the tagged version of AN8D showed little, if any, increase in soluble protein (Figure 4A, lanes 5 and 6). AQ14R was atypical, having a strong phenotype, yet little soluble protein and decreased protein levels (Figure 4A, lanes 7 and 8). We also examined whether expression of the ASU and PNM mutants led to solubilization of WT Sup35p in [*PSI*$^+$] yeast by coexpressing HA-tagged WT Sup35p and untagged mutant proteins. Though most ASU mutants did not result in an increase in soluble WT Sup35p, expression of AS17R led to significant solubilization of WT protein (Figure 4C, lanes 3 and 4). The PNM mutants generally caused a modest increase in soluble WT protein with the strongest effect resulting from expression of PQ24R (Figure 4C, lanes 5 and 6).

WT Sup35 PrD Rapidly Forms Amyloids In Vitro in a Reaction that Has Both Concentration-Dependent and -Independent Phases

Recently, three groups demonstrated that the PrD domain from Sup35p can form self-propagating aggregates in vitro (Glover et al., 1997; King et al., 1997; Paushkin et al., 1997), facilitating greatly detailed studies of the mechanism of fibril formation. Although in all of these studies amyloid formation was preceded by a lag phase that was eliminated by the addition of preformed fibrils, there were dramatic differences in the time scale of conversion. In particular, Ter-Avanesyan and coworkers (Paushkin et al., 1997) observed that in cell-free extracts undergoing a constant slow rotation, a protein containing the PrD and M domains (PrD−M) was recruited into preformed aggregates within 2 hr. In contrast, Lindquist and coworkers found that pure PrD-M formed amyloids slowly: spontaneous conversion took days, and seeded conversion took ~20 hr (Glover et al., 1997). Initially, we observed that in unrotated reactions pure PrD-M converted slowly even in the presence of preformed fibrils, although the conversion reaction was complicated by amorphous aggregation and settling of fibrils during long incubation times.

These difficulties could be minimized by slowly rotating the samples during the incubation. Rotation also caused a dramatic increase in the conversion kinetics, as detected by Congo red binding, with seeded reactions going to completion in as little as 45 min and unseeded reactions within 180 min (Figure 5A). As judged by gel filtration, all of the monomeric starting material appears to have converted to higher order oligomeric forms. We also observed structural changes on this time scale, such as increased β−sheet content by circular dichroism (data not shown). Finally, EM and AFM analyses directly confirmed that the conversion results in fibril formation (Figure 5B and data not shown). Although amyloids observed by AFM were similar in dimensions and general features to those seen by EM (Glover et al., 1997; King et al., 1997), this analysis revealed several novel features. For example, we saw fibrils containing a prominent ~10 nm ridge along the filament axis as well as branching fibrils and fibrils emanating from globular structures (Figure 5B). Branching fibrils were also recently observed in AFM analysis of β-amyloid protein filaments (Harper et al., 1997b) and could be important for creating new fibrils during amyloid propagation.

The rapid and reproducible kinetics of conversion allowed us to perform quantitative analyses of fibril formation. The conversion kinetics can be characterized by

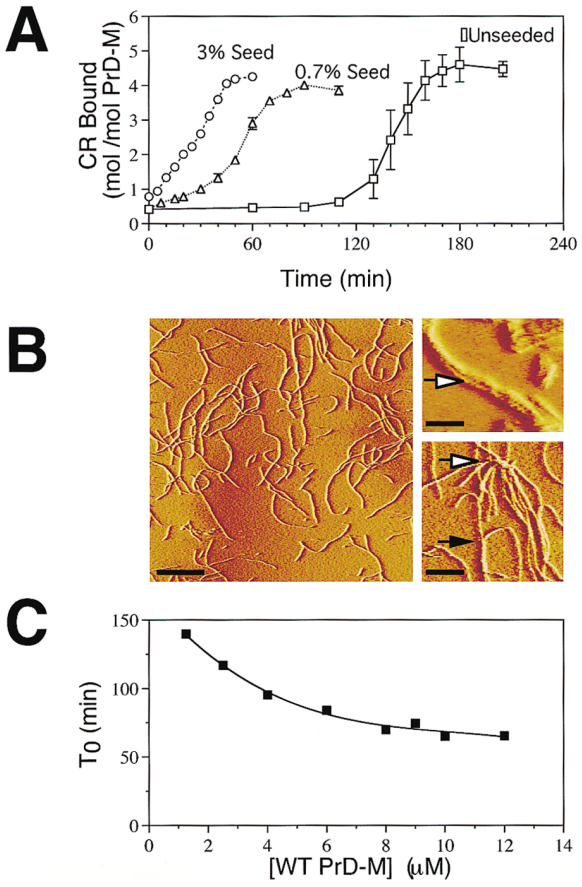

Figure 5. In Vitro Amyloid Fibril Formation of WT Sup35p

To initiate conversion, concentrated protein in urea was diluted at least 100-fold into buffer C and subjected to continuous slow rotation. At the indicated times, the extent of fibril formation was assayed by Congo red (CR) binding. Each time curve was performed at least three times, unless noted otherwise. Errors larger than the size of symbols are indicated by bars.

(A) Kinetics of conversion of 2.5 μM WT PrD-M in absence (square) and presence of 0.7% (wt/wt) (triangle) and 3% (wt/wt) (circle) preformed WT fibril. The kinetics of WT seeded with 3% (wt/wt) fibril were done in duplicate.

(B) Atomic force micrograph of WT PrD-M amyloids. Examples of a fibrillar ridge (open arrow) are seen in the top right panel. In the bottom right panel, an amorphous structure from which many fibrils emanate (open arrow) and branching fibrils (closed arrow) are highlighted. Scale bars are 1 μm, except for upper right figure (100 nm).

(C) Effect of concentration on the lag phase (T_0) of WT Sup35. T_0 is calculated as described in Experimental Procedures.

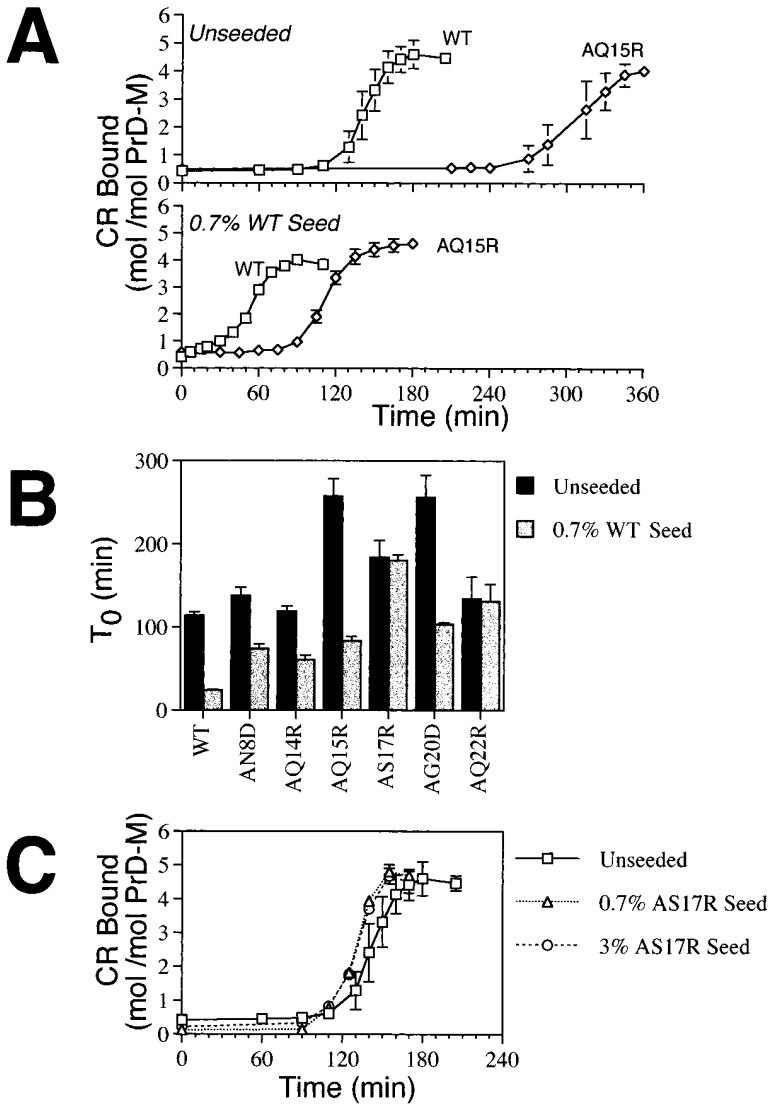

Figure 6. Effects of ASU Mutations on the Kinetics of Amyloid Fibril Formation

Amyloid formation was monitored by examining Congo red (CR) binding as a function of conversion time. Errors larger than the size of symbols are indicated by bars.

(A) Comparison of amyloid fibril formation between a representative ASU mutant (AQ15R) and WT PrD-M either in the absence (upper panel) or presence (lower panel) of 0.7 % (wt/wt) WT fibril.

(B) Summary of the lag phases (T_0) in amyloid formation for the ASU mutants either in the absence (black bar) or presence (shaded bar) of 0.7% (wt/wt) WT fibril. Note the failure of WT fibrils to accelerate conversions of AS17R and AQ22R.

(C) Conversion kinetics of WT PrD-M in the presence of 0% (circle), 0.7% (square), and 3% (diamond) (wt/wt) AS17R fibrils.

two terms: a lag time (T_0), the time prior to the increase in Congo red binding, and a conversion time (T_c), the time between initiation of conversion and its completion. At 2.5 μM, PrD-M has a lag time of 114 ± 4 min and a conversion time of 53 ± 12 min (Figure 5A). To eliminate contaminating preformed fibrils, urea-denatured PrD-M (30 kDa) was passed through a 100 kDa filter prior to initiation of conversion. This filtration step appeared to be sufficient, as passage through a 50 kDa filter immediately after dilution from denaturant did not affect the conversion kinetics (data not shown). Addition of increasing amounts of preformed fibrils accelerated conversion by decreasing T_0 without significantly changing T_c. For example, 0.7% (wt/wt) fibrils shortened the T_0 to 24 ± 1 min, and 3% (wt/wt) fibrils eliminated the lag time completely (Figure 5A).

Using the in vitro assay, we probed the nature of the rate-limiting step responsible for the lag phase. In particular, is this lag due to the cooperative formation of an ordered oligomeric nucleus as suggested by the nucleation-polymerization model (Jarrett and Lansbury, 1993)? Because the seed is oligomeric, the nucleation model predicts that the lag time will show a strong concentration dependence that approaches zero at high concentrations. We found that within a range of 1.25–6 μM, increasing PrD-M concentration did lead to a modest (~2-fold) decrease in lag time (Figure 5C). Further increases in PrD-M concentration, however, did not lead to a further decrease of T_0 to below 65 min. Thus, at concentrations above 6 μM, the rate-limiting step in conversion is unaffected by protein concentration. Importantly, the molar fraction of Congo red bound also did not change significantly over the observed concentration range (1.25–12 μM).

Purified Mutant ASU Proteins Show Decreased Rates of Amyloid Formation In Vitro

We next examined the kinetics of de novo amyloid formation for the ASU mutants. A representative conversion curve of an ASU mutant (AQ15R) reveals a marked decrease in conversion kinetics compared to WT PrD-M (Figure 6A). As with the other mutants, the slow rate of

fibril formation of AQ15R was predominantly attributable to an increase in lag time ($T_0 = 260 \pm 20$ min vs. 114 ± 4 min for WT) rather than a change in T_c. A summary of T_0 of all the mutants is shown in Figure 6B. Significantly, the mutants that showed the lowest solubility in vivo (AN8D and AQ14R) had T_0 values comparable to that of WT protein, whereas the stronger mutants (AS17R, AQ15R, and AG20D) showed significantly larger T_0 values.

To simulate amyloid propagation in vivo, we examined the ability of preformed WT PrD-M fibrils to promote the conversion of purified ASU mutant proteins. For 4 of the 6 ASU mutants, addition of WT fibrils did accelerate the conversion kinetics. However, the rate of seeded conversion was significantly slower for all of the ASU mutants than for WT (Figure 6B). For example, in the presence of 0.7% (wt/wt) WT fibrils, the T_0 of AQ15R was 83 ± 5 min as compared to 24 ± 1 min for WT. Interestingly, for two of the mutants with the strongest in vivo phenotype, AS17R and AQ22R, addition of WT fibrils did not increase the rate of amyloid formation, even though AQ22R showed only a modest defect in de novo fibril formation. Intringuingly, we also found that AS17R mutant fibrils fail to seed the conversion of WT Sup35p (Figure 6C).

The N-Terminal Region of the PrD Identified by Mutagenesis Can Be Functionally Replaced with PolyGln

Gln and Asn residues are chemically similar, differing solely by a single carbon atom separating the carboxyamide group from the backbone. Although the Ser side chain does not have a hydrogen bond acceptor like a carboxyamide side chain, it is a polar group with a hydrogen bond donor. To test the functional equivalence of these side chains, we made a series of glutamine replacement variants (GRV) of the Sup35p PrD (Figure 7). In the first set of variants, termed GRV(+Gly) and GRV(−Gly), all of the residues in the N-terminal region of the PrD that were identified by mutagenesis, either including or not including the single Gly, respectively, were replaced with Gln. A second set of variants, termed GRV(polyQ+Gly) and GRV(polyQ-Gly) were made in which all of the residues (amino acids 8–24) in the N-terminal region, either including or not including the single Gly, were replaced with Gln. These domains were fused to GFP and put under the control of the CUP1 promoter.

We examined the aggregation state of the GRV-GFP fusion proteins in [*PSI*$^+$] or [*psi*$^-$] yeast as a function of expression time. The behavior of the GRV(−Gly) variant was indistinguishable from WT PrD. In [*PSI*$^+$] cells, GRV(-Gly)-GFP showed punctate fluorescence even at early points in the induction (3 hr), whereas only diffuse staining was observed in [*psi*$^-$] cells (Figure 7). For GRV(+Gly), at early times the fluorescent pattern in [*PSI*$^+$] cells appeared diffuse in a significant fraction of the cells. At later times, however, a uniformly punctate pattern was observed. This indicates that GRV(+Gly)-GFP was also capable of being recruited in WT aggregates although with decreased efficiency compared to GRV(-Gly)-GFP. The behavior of the GRV[polyQ-Gly] and GRV[polyQ+Gly] was comparable to GRV[−Gly] and GRV[+Gly], respectively, indicating that replacement of the N-terminal residues not identified by mutagenesis had little effect on function of the PrD (Figure 7 and data not shown). Intriguingly, GRV(+Gly) retained its ability to form de novo aggregates, as even at early expression times a small fraction (~1%) of the [*psi*$^-$] cells showed a punctate fluorescence pattern. At longer incubation times, this fraction increased to ~25%. These aggregates are likely to represent, at least in part, genuine conversion events, as overexpression of either GRV-GFP fusion in [*psi*$^-$] cells resulted in a enhanced rate of conversion to [*PSI*$^+$] state. Taken together, these observations indicate that even after replacement of the N-terminal Gln/Asn region with a polyGln stretch, the PrD retained its ability both to form new aggregates and to be recruited into existing aggregates.

Discussion

Even though the association of amyloid fibrils with diseases has been appreciated for several decades, little is known about what makes a protein amyloidogenic. The cytoplasmically inherited [*PSI*$^+$] factor of yeast provides a powerful system for studying amyloid formation in vivo and in vitro. Here, we have exploited the PSI phenomenon to identify point mutations in the prion-determining domain (PrD) of Sup35p that are defective in amyloid formation and propagation. This work differs fundamentally from previous genetic studies of mammalian amyloid disorders that have relied on identification of naturally occurring mutations which accelerate disease. Such mutations typically increase the propensity to form amyloids by destabilizing the native state and thus do not report directly on the requirements for amyloid formation (Kelly et al., 1997; Wetzel, 1997).

The mutants that we have identified allowed us both to define the sequence requirements for Sup35p amyloid formation in vivo and to test the relevance of in vitro conversion reactions. Two classes of mutants that lead to increased levels of soluble protein were identified: the first (ASU) inhibited incorporation into aggregates without irreversibly preventing propagation of WT amyloids, and the second (PNM) resulted in curing of the [*PSI*$^+$] state in addition to its ASU phenotype. In vitro conversion reactions using pure ASU-PrD proteins indicate that the increased solubility of these mutants is caused directly by a defect in recruitment of soluble protein by WT prion-like amyloids. We are currently investigating the molecular basis of the curing by the PNM mutants.

Our studies reveal a critical role for Gln and Asn residues in stabilization of the amyloid state. First, all of the mutations cluster to the most Gln/Asn-rich region of the Sup35p PrD. Second, all of the mutations were found in Gln or Asn residues, with the exception of a single Ser and a single Gly. Finally, when present in the context of full-length Sup35p, this region can be replaced by a polyGln tract while retaining its ability both to form de novo amyloids and to be incorporated into preexisting WT amyloids. These observations argue for the functional equivalence of the various polar residues (Gln,

```
                    * * *  *  * *  * *  *  *  *
WT          M S D S N Q G N N Q Q N Y Q Q Y S Q N G N Q Q Q G
GRV(+G)     - - - - - - - Q Q Q Q Q - Q Q - Q Q - Q - Q Q Q -
GRV(-G)     - - - - - - - Q Q Q Q Q - Q Q - Q Q - G - Q Q Q -
GRV(pQ-G) - - - - - Q - Q Q Q Q Q Q Q Q Q Q Q G Q Q Q Q -
```

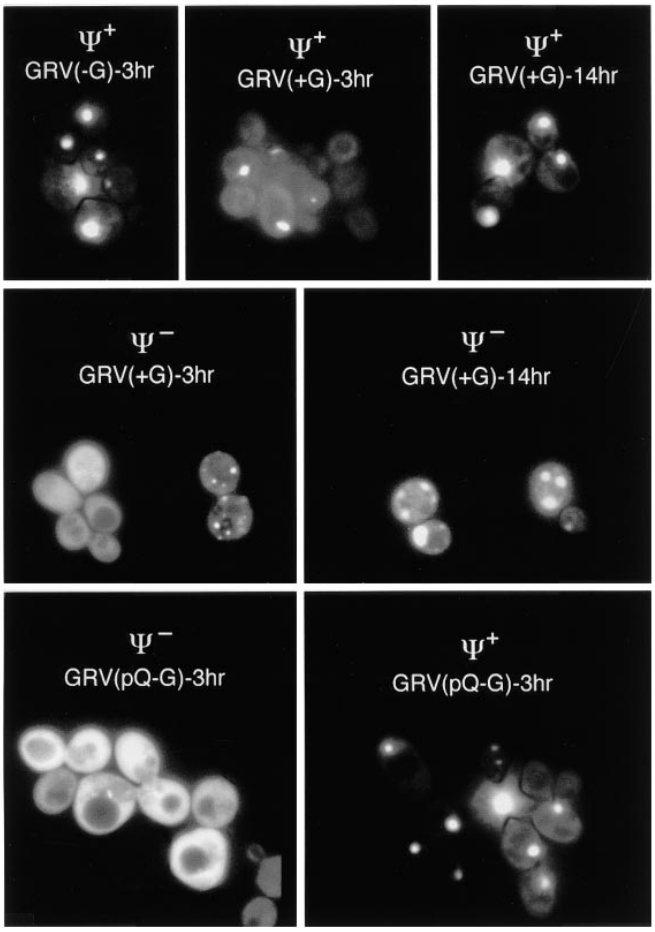

Figure 7. Recruitment of GRV Alleles of Sup35p by WT Aggregates

Yeast expressing GRV-GFP fusion proteins were examined at the indicated time after induction. The PSI state of the cells and the expressed GRV allele are as noted. The amino acid changes, relative to WT, in the various GRV alleles are indicated in top panel. Amino acids altered in ASU or PNM mutants are denoted by an asterisk.

Asn, and Ser) in this critical region of the Sup35p PrD. A possible explanation for the stabilization of the amyloid state by Gln/Asn residues was suggested by Perutz and coworkers, who pointed out that in β sheets carboxyamide side chains could form a "polar zipper" involving a network of side chain–main chain hydrogen bonds (Stott et al., 1995).

It is likely that Gln- and Asn-rich domains play an important role in stabilizing a significant subset of amyloid phenomena. The putative PrD region of the Sup35p homolog of *Pichia pinus* is rich in Asn and Gln, despite the lack of linear sequence homology with the *S. cerevisiae* gene (Kushnirov et al., 1990). Even more striking is the recently sequenced *SUP35* gene from *Candida albicans*, which contains ~55 Gln residues in its putative PrD domain, including long stretches of pure Gln repeats near the N terminus. These observations suggest that the amino acid composition of a protein, as much as its exact primary sequence, determines its amyloidogenicity. Another epigenetic factor in yeast, [*URE3*], also appears to propagate by a prion-like mechanism (Wickner, 1994). The protein responsible for the [*URE3*] state, Ure2p, is extremely rich in Asn as well as other polar residues. Furthermore, Ure2p has been reported to form filaments in vitro (King et al., 1997). Perhaps most interestingly, a number of neurodegenerative diseases have recently been found to result from expansion of polyGln repeats that leads to intracellular aggregates in vivo and amyloids in vitro (see below).

Implications for the Prion Hypothesis

The prion hypothesis argues that a protein alone can act as an infectious agent, leading to a permanent change in the phenotype of the infected organism (Prusiner et al., 1998). This infectivity is thought to result from an altered conformation that both causes the phenotypic change and promotes conversion of new protein, thereby allowing self-replication. Studies on the mammalian prion protein PrP, the yeast prion Sup35p, and nonprion amyloids have reproduced self-propagating conformational changes in

vitro (Glover et al., 1997; Harper and Lansbury, 1997; King et al., 1997; Paushkin et al., 1997). Connecting these conformational changes to the phenotypic change, however, has proven more elusive. Here, we show that pure PrD can propagate amyloids on a physiological time scale in vitro. Moreover, we used a series of point mutants that lead to a loss of the prion-associated phenotype to test the relevance of the in vitro conversion reaction. These mutants cause solubilization of protein in vivo and decreased rates of de novo amyloid formation and recruitment into preformed fibrils in vitro. These observations provide perhaps the most compelling data to date linking an in vitro conversion reaction to the phenotypic change effected by a prion, thus providing strong support for the prion hypothesis.

The studies also furnish insights into the mechanism by which the Sup35p prion propagates its altered conformation. In vitro characterizations of the kinetics of amyloid formation from purified amyloidogenic proteins or peptides have suggested that conversion is a nucleation-dependent process (Jarrett and Lansbury, 1993; Harper and Lansbury, 1997). In such processes, the lag phase results from the thermodynamically unfavorable formation of competent nuclei and is followed by a conversion phase in which the transition from monomer to fibril occurs in a rapid, cooperative fashion. The nucleation-polymerization model makes several predictions (Jarrett and Lansbury, 1993) that distinguish it from other conversion mechanisms (e.g., the template conversion model in which the catalyst acts by promoting a rate-limiting conformational change [Prusiner and al, 1998]). First, there is a critical monomer concentration below which no conversion occurs. Second, the length of the lag time is highly dependent on the protein concentration. Finally, the lag phase will approach zero at infinite concentration, and as this limit is approached, addition of seed no longer accelerates fiber formation.

Here, we tested critically the nucleation-polymerization model by examining the kinetics of de novo amyloid formation of Sup35p. We find that within a range of 1.25–12 μM the conversion of monomer appears to go to completion. Thus, the critical concentration, if it exists, is well below micromolar as compared to 10–40 μM for β-amyloid peptide (Harper and Lansbury, 1997). We also find that the rate of amyloid formation shows only modest concentration dependence. In particular, between 1.25 and 6 μM the rate of spontaneous conversion is approximately first order. At concentrations between 6 and 12 μM, the lag time has a constant value of $\sim$65 min. Yet this lag phase is completely eliminated by addition of as little as 3% (wt/wt) preformed aggregate. It remains possible that at extremely low concentrations, the kinetics of conversion would be adequately described by the nucleation polymerization model. However, we find dramatic catalysis of fibril formation even at concentrations where oligomerization is not rate limiting. These data argue that fibrils accelerate the conversion of Sup35p by promoting a conformational change (e.g., conversion of profibrils to fibrils [Harper et al, 1997a]) rather than solely by providing a multimeric nucleus.

Although pure Sup35p PrD-M forms amyloids rapidly in vitro, a variety of cellular factors are likely to play an important role in propagation of the Sup35p prion state. For example, the molecular chaperone HSP104 is required for maintenance of the [*PSI*$^+$] state; paradoxically, HSP104 also causes loss of [*PSI*$^+$] when overexpressed (Chernoff et al., 1995). We find that the kinetics of conversion are enhanced greatly by the addition of a slow rotation step. Similar enhancement in the kinetics of polymerization is observed when hemoglobin S is subjected to rotation forces (Briehl, 1980). Given that in the absence of such forces, conversion of Sup35p in vitro is far slower than the doubling time of yeast, it is an attractive hypothesis that in a growing cell amyloid fibrils undergo continuous disrupton. As noted by Ter-Avanesyan and coworkers, HSP104 might contribute to such an effect, as it has been shown to break up other protein aggregates (Paushkin et al., 1996; see, however, Patino et al., 1996). Using the in vitro assay, we can quantitatively assess the ability of HSP104 or other cellular components to increase the number of polymerizing ends in an amyloid fibril sample.

A molecular chaperone, termed protein X, has also been implicated in propagation of the prion form of the mammalian PrP protein (Kaneko et al., 1997). The identity of protein X is unknown, but its existence has been inferred by the behavior of a number of dominant-negative forms of PrP. Our dominant-negative Sup35p alleles could also result from altered recognition by a molecular chaperone such a HSP104. Alternatively, our Sup35p mutants might form heteropolymers with WT protein that fail to effectively promote conversion of either WT or mutant protein. Consistent with this proposal, GFP analysis reveals that the mutants can be recruited into WT aggregates in vivo. Moreover, in vitro WT and AS17R amyloids are mutually defective in seeding each other's conversion.

Implications for the Mechanism of CAG Repeat–Mediated Pathogenesis: PolyGln Diseases as Intracellular Prions?

A number of inherited neurodegenerative diseases result from expansion of the CAG nucleotide triplet leading to the insertion of a polyGln tract at the protein level. Concurrent with our studies, polyGln insertions were shown to lead to formation of amyloid fibrils in vitro and in vivo (e.g., Paulson et al., 1997; Scherzinger et al., 1997; see, however, Kahlem et al., 1998). This polyGln-mediated aggregation appears to be intimately associated with pathogenesis.

Our functional analysis of Sup35p amyloid formation raises the interesting possibility that [*PSI*$^+$] and polyGln-mediated pathogenesis are related phenomena involving intracellular prion-like propagation of amyloid fibrils stabilized by a polar network of carboxyamide side chains. There are, however, important differences between the aggregation of Sup35p- and polyGln-mediated amyloid formation. Notably, while the total number of Gln/Asn residues in Sup35p is comparable to the number found in the pathogenic repeat disorders, the Gln/Asn tracts in Sup35p are not continuous. There is also currently no direct evidence to address whether polyGln amyloids facilitate their own conversion during pathogenesis. A prediction of the self-replicating amyloid model is that a cell will undergo a stochastic conversion event, after which newly made protein will be recruited into amyloid fibrils. Consistent with this, we

found in a related set of studies that huntingtin protein containing pathogenically expanded polyGln repeats fused to GFP is initially soluble when expressed in yeast but eventually forms aggregates that appear to propagate stably (A. S. and J. S. W., unpublished data). We are currently using the in vitro assay to directly examine the propagation of huntingtin amyloids.

Regardless of the exact mechanism of propagation, yeast could provide a powerful genetic system for studying polyGln-mediated amyloid formation. In particular, yeast should facilitate efforts to find extragenic factors involved in the conversion process (e.g., molecular chaperones, transglutaminases, or proteolytic processing enzymes). Indeed, as with Sup35p, increased HSP104 levels slow somewhat the rate of huntingtin aggregation (A. S. and J. S. W., unpublished data). Finally, by using yeast it should be possible to rapidly screen for dominant-negative mutants or small molecules capable of inhibiting the conversion process in vivo.

Experimental Procedures

General Procedures and Reagents

Isogenic [*PSI*$^+$] and [*psi*$^-$] versions of strain 74D-694 [*MATa*, *ade1*, *his3*, *leu2*, *trp1*, *ura3*; suppressible marker *ade1-14(UGA)*] were used (Chernoff et al., 1995). All nucleic acid and yeast manipulations were performed according to standard laboratory protocols (Sherman, 1991; Ausubel et al., 1995). PCR primers were as follows: P1, GGCCCCCCTCGAGTGAGAGAACCGTTAAATTCCC; P2, CCCCGGATCCTGCTAGTGGGCAGATATAGAT; P3, GGGAGGCTCGAGCTTCAACGATTTCTATGATTC; P4, GGGGGATCCTATGTGATGATTGATTGATTG; P5, GCGGGATCCACAATGTCGGATTCAAACCA; P6, CCGGCCGAATTCAGATCTATCGTTAAC; P7, CCCCCCAGATCTGAATTCCCATGGATGTTTGGTGGTAAAGATCAC; P8, CCCCCGAGCTCACCTTGTTTATGGTATATGGT; P9, GGGGGGGCATATGTCGGATTCAAACCAAGGC; P10, CCGGGACGCGTGAATTCTTAATGGTGGTGATGGTGATGGTGATGATGATCGTTAACAACTTCGTCATC-. *S. Cerevisiae* Genomic DNA was used as a PCR template (Stratagene).

Plasmid Construction

To facilitate exchange of promoters and protein domains, PCR was used to introduce restriction sites flanking the promoter, the PrD-M domain, and the EF domain of *SUP35*, generating a set of interchangeable cassettes. The promoter cassette was defined by a 5′ XhoI site and a 3′ BamH1 site, the PrD-M cassette by a 5′ BamH1 site and 3′ BglII and EcoR1 sites, and the EF cassette by a 5′ EcoR1 site and a 3′ SacI site. Two promoters were used: the endogenous *SUP35* promoter (Sp) (P1 and P2) and the *CUP1* promoter (Cp) (P3 and P4). PrD-M domains were generated by P5 and P6. The EF domain was generated using P7 and P8. This domain was exchanged with GFP where indicated; GFP containing the appropriate sites was derived from pRS316-Pho4-GFP (E. K. O'Shea, personal communication). Epitope tags were inserted between the M and EF domains, using the 5′ BglII site and the 3′ EcoR1 site. All plasmids were derived by ligating the insert between the Xho1/Sac1 sites of the following vectors; pRS316 (low copy CEN/ARS, *URA3*+), pRS315 (low copy CEN/ARS, *LEU2*+), and pRS426 (high copy 2 μm, URA3+) (Christianson et al., 1992). Constructs are denoted by the plasmid backbone, promoter, PrD allele, and whether the EF or GFP domain is present (Epitope tags are noted between the PrD-M and EF domains where relevant). For bacterial expression, the appropriate allele of PrD-M was amplified using P9 and P10, which introduces a His tag at the C terminus. These products were subcloned into NdeI/EcoRI sites of a T7 expression vector. The sequence of all plasmids was confirmed by dye termination sequencing (Perkin Elmer).

Screen for ASU and PNM Mutants

The SUP35 PrD was mutagenized by 30 rounds of PCR amplification with Taq polymerase using the manufacturer's conditions and P1 and P6. Diversity in the mutant pool was maintained by keeping 3–6 separate PCR pools and 3–6 separate transformation pools. Based on the levels of incidental second site mutations as well as sequencing of phenotypically WT PrD alleles, we estimate that ~30% of the PCR products contain at least one point mutation. The mutagenized PrD was reintroduced into p316SpSUP-EF by cotransforming [*PSI*$^+$] yeast with the linear PCR product and p316SpSUP-EF gapped by digestion with BamHI and PflmI. Transformants were selected on SD-URA, harvested by washing in TE, and plated at density of 500 cells/plate on YPD to test for sectoring. The sectoring colonies were patched onto SD-URA, retested for sectoring by growth on YPD, tested for plasmid-dependent antisuppression by growth on SD-URA, ADE, and SD-URA, and tested for curing by growth on SD-URA supplemented with 5-FOA.

GFP Induction/Microscopy and Extract Preparation/High Speed Centrifugation

Yeast carrying p426CpSUP-GFP, p426CpASU/PNM-GFP (11 alleles), or p426CpGRV-GFP (4 alleles) were grown to early log phase in SD-URA. At the indicated time after induction with 50 μM $CuSO_4$, samples were spun down, resuspended in TE and examined by fluorescence microscopy (Olympus BX60), and photographed by film or CCD camera (Photometrics).

To prepare extracts, 50 ml cultures of yeast carrying either p316SpSUP$_{(HA)3}$EF, p316SpASU/PNM$_{(HA)3}$EF, or p315SpSUP$_{(HA)3}$EF and p316SpASU/PNM-EF were grown in appropriate selective medium to mid–log phase and harvested at room temperature. Cell pellets were washed once in an equal volume of distilled water and resuspended in buffer A (25 mM Tris-HCl [pH 7.5], 50 mM KCl, 10 mM $MgCl_2$, 1 mM EDTA, 5% Glycerol, 1 mM PMSF, 2 μg/ml pepstatin and leupeptin, and 100 μg/ml ribonuclease A). Cell pellets were resuspended in approximately 2 vol of buffer A, 2 vol of glass beads were added, and cells were disrupted by vortexing for 3 min at 4°C. Centrifugation was performed as described (Patino et al., 1996) with minor modifications. The slurries were spun at 8000 g for 3 min at 4°C to pellet unbroken cells and glass beads; the remaining supernatant was spun at 100,000 g for 30 min at 4°C. Supernatant was removed, and the pellet was resuspended in an equal volume of cold buffer A. Samples (20 μg of total protein) were analyzed by SDS-PAGE and Western blot analysis (Ausubel et al., 1995) using the 16B12 antibody (Babco) and goat anti-mouse IgG-HRP conjugate (Bio-Rad).

PrD-M Expression and Purification

Pure PrD-M was prepared largely as described previously (Glover et al., 1997). Briefly, cell pellets from 1–2 l of growth were lysed in 30 ml of buffer B (25 mM Tris [pH 7.8], 300 mM NaCl, 6 M urea). Subsequent to centrifugation at 25,000 g (20 min), the supernatant was filtered by 0.22 μm filter (Millipore) and applied to 20 ml Ni-NTA agarose (Qiagen) column. The column was washed with 5 column vol buffer B and eluted with a pH gradient in same buffer without NaCl. Pooled fractions were applied to a 30 ml Source 15S column (Pharmacia) equilibrated in 50 mM MES [pH 6.0], 6 M urea and eluted with 0–400 mM NaCl gradient in the same buffer. Pure PrD-M was concentrated with centricon-10 (Amicon), filtered by microcon-100 (Amicon), aliquoted, and stored at −80°C. Protein concentration was determined by UV absorption at 275 nm.

Congo Red Binding Assay

Congo red binding assays were carried out largely as described previously (Klunk et al., 1989). Congo red (Sigma) was dissolved in buffer C (5 mM potassium phosphate, 150 mM NaCl), filtered with 0.22 μm filter (Millipore), and adjusted to 100 mM. To initiate conversion, concentrated PrD-M was diluted at least 100-fold into buffer C in 2 ml microcentrifuge tubes at room temperature. The solution was subjected to constant rotation (7.5 rpm) using a RKVS Rotamix (ATR). At indicated times, protein was diluted to 2 μM in the presence of 10 μM Congo red in buffer C. Absorbances at 540 and 477 nm were determined (either by Shimadzu UV160U or Aviv 14DS spectrophotometer). Congo red bound per mole of PrD-M was determined by the formula $(A_{540}/25292)-(A_{477}/46306)$. Quantitative measurement of the length of the lag phase (T_0) was performed by fitting the middle of the sigmoidal curves with a straight line and solving the time for

which the amount of Congo red bound is that of baseline. Likewise, the length of the conversion phase (T_c) was calculated by subtracting T_0 from the time at which dye binding is maximal.

Atomic Force Microscopy

Protein samples were absorbed to freshly cleaved mica surface. AFM images were collected with a NanoScope IIa (Digital Instruments) operated in contact mode with a commercial NP-S silicon nitride tips.

Acknowledgments

We are grateful to Y. Chernoff for providing yeast strains; E. Wanker for providing Huntingtin plasmids; and F. Cohen, I. Herskowitz, J. Kelly, and members of the Lim and Weissman labs for helpful discussions. This work was supported by a Howard Hughes Medical Institute Predoctoral Fellowship (A. H. D.) and grants from the Howard Hughes Medical Institute, the David and Lucile Packard Foundation, and the Searle Scholars Program.

Received April 8, 1998; revised May 5, 1998.

References

Ausubel, F.M., Brent, R., Kingston, R.C., Moore, R.D., Seidman, J.G., Smith, J.A., and Struhl, K. (1995). Current Protocols in Molecular Biology (New York: John Wiley and Sons, Inc.).

Briehl, R.W. (1980). Solid-like behaviour of unsheared sickle haemoglobin gels and the effects of shear. Nature *288*, 622–624.

Caughey, B., and Chesebro, B. (1997). Prion protein and the transmissible spongiform encephalopathies. Trends Cell. Biol. *7*, 56–62.

Chernoff, Y.O., Lindquist, S.L., Ono, B., Inge-Vechtomov, S.G., and Liebman, S.W. (1995). Role of the chaperone protein Hsp104 in propagation of the yeast prion-like factor [psi+]. Science *268*, 880–884.

Christianson, T.W., Sikorski, R.S., Dante, M., Shero, J.H., and Hieter, P. (1992). Multifunctional yeast high-copy-number shuttle vectors. Gene *110*, 119–122.

Cox, B.S., Tuite, M.F., and McLaughlin, C.S. (1988). The psi factor of yeast: a problem in inheritance. Yeast *4*, 159–178.

Doel, S.M., McCready, S.J., Nierras, C.R., and Cox, B.S. (1994). The dominant PNM2- mutation which eliminates the psi factor of Saccharomyces cerevisiae is the result of a missense mutation in the SUP35 gene. Genetics *137*, 659–670.

Glover, J., Kowal, A., Schirmer, E., Patino, M., Liu, J., and Lindquist, S. (1997). Self-seeded fibers formed by Sup35, the protein determinant of [PSI+], a heritable prion-like factor of *S. cerevisiae*. Cell *89*, 811–819.

Harper, J.D., and Lansbury, P.T., Jr. (1997). Models of amyloid seeding in Alzheimer's disease and scrapie: mechanistic truths and physiological consequences of the time-dependent solubility of amyloid proteins. Annu. Rev. Biochem. *66*, 385–407.

Harper, J.D., Wong, S.S., Lieber, C.M., and Lansbury, P.T. (1997a). Observation of metastable Abeta amyloid protofibrils by atomic force microscopy. Chem. Biol. *4*, 119–125.

Harper, J.D., Lieber, C.M., and Lansbury, P.T., Jr. (1997b). Atomic force microscopic imaging of seeded fibril formation and fibril branching by the Alzheimer's disease amyloid-beta protein. Chem. Biol. *4*, 951–959.

Jaenicke, R., and Seckler, R. (1997). Protein misassembly in vitro. Adv. Protein Chem. *50*, 1–59.

Jahlem, P., Green, H., and Djian, P. (1998). Transglutaminase action imitates Huntingtin's disease: selective polymerization of Huntingtin containing expanded polyglutamine. Mol. Cell *1*, 595–601.

Jarrett, J.T., and Lansbury, P.T.J. (1993). Seeding "one-dimensional crystallization" of amyloid: a pathogenic mechanism in Alzheimer's disease and scrapie? Cell *73*, 1055–1058.

Kaneko, K., Zulianello, L., Scott, M., Cooper, C.M., Wallace, A.C., James, T.L., Cohen, F.E., and Prusiner, S.B. (1997). Evidence for protein X binding to a discontinuous epitope on the cellular prion protein during scrapie prion propagation. Proc. Natl. Acad. Sci. USA *94*, 10069–10074.

Kelly, J.W., Colon, W., Lai, Z., Lashuel, H.A., McCulloch, J., McCutchen, S.L., Miroy, G.J., and Peterson, S.A. (1997). Transthyretin quaternary and tertiary structural changes facilitate misassembly into amyloid. Adv. Protein Chem. *50*, 161–181.

King, C.Y., Tittmann, P., Gross, H., Gebert, R., Aebi, M., and Wüthrich, K. (1997). Prion-inducing domain 2-114 of yeast Sup35 protein transforms in vitro into amyloid-like filaments. Proc. Natl. Acad. Sci. USA *94*, 6618–6622.

Klunk, W.E., Pettegrew, J.W., and Abraham, D.J. (1989). Two simple methods for quantitating low-affinity dye-substrate binding. J. Histochem. Cytochem. *37*, 1293–1297.

Kushnirov, V., Ter-Avanesyan, M., Didichenko, S., Smirnov, V., Chernoff, Y., Derkach, I., Novikova, O., Inge-Vechtomov, S., Neistat, M., and Tolstorukov, I. (1990). Divergence and conservation of SUP2 (SUP35) gene of yeast Pichia pinus and Saccharomyces cerevisiae. Yeast *6*, 461–472.

Lansbury, P.T., Jr., Costa, P.R., Griffiths, J.M., Simon, E.J., Auger, M., Halverson, K.J., Kocisko, D.A., Hendsch, Z.S., Ashburn, T.T., Spencer, R.G., et al. (1995). Structural model for the beta-amyloid fibril based on interstrand alignment of an antiparallel-sheet comprising a C-terminal peptide. Nat. Struct. Biol. *2*, 990–998.

Lazo, N.D., and Downing, D.T. (1998). Amyloid fibrils may be assembled from beta-helical protofibrils. Biochemistry *37*, 1731–1735.

Lindquist, S. (1997). Mad cows meet psi-chotic yeast: the expansion of the prion hypothesis. Cell *89*, 495–498.

Liu, Y., Hart, P.J., Schlunegger, M.P., and Eisenberg, D. (1998). The crystal structure of a 3D domain-swapped dimer of RNaseA at 2.1Å resolution. Proc. Natl. Acad. Sci. USA *95*, 3437–3442.

Patino, M., Liu, J., Glover, J., and Lindquist, S. (1996). Support for the prion hypothesis for inheritance of a phenotypic trait in yeast. Science *273*, 622–626.

Paulson, H.L., Perez, M.K., Trottier, Y., Trojanowski, J.Q., Subramony, S.H., Das, S.S., Vig, P., Mandel, J.-L., Fischbeck, K.H., and Pittman, R.N. (1997). Intranuclear inclusions of expanded polyglutamine protein in spinocerebellar ataxia type 3. Neuron *19*, 333–344.

Paushkin, S.V., Kushnirov, V.V., Smirnov, V.N., and Ter-Avanesyan, M.D. (1996). Propagation of the yeast prion-like [psi+] determinant is mediated by oligomerization of the SUP35-encoded polypeptide chain release factor. EMBO J. *15*, 3127–3134.

Paushkin, S., Kushnirov, V., Smirnov, V., and Ter-Avanesyan, M. (1997). In vitro propagation of the prion-like state of yeast Sup35 protein. Science *277*, 381–383.

Prusiner, S.B., Scott, M.R., DeArmond, S.J., and Cohen, F.E. (1998). Prion protein biology. Cell *93*, 337–348.

Scherzinger, E., Lurz, R., Turmaine, M., Mangiarini, L., Hollenbach, B., Hasenbank, R., Bates, G.P., Davies, S.W., Lehrach, H., and Wanker, E.E. (1997). Huntingtin-encoded polyglutamine expansions form amyloid-like protein aggregates in vitro and in vivo. Cell *90*, 549–558.

Sherman, F, (1991). Getting started with yeast. Meth. Enzymol. *194*, 3–21.

Stansfield, I., Jones, K.M., Kushnirov, V.V., Dagkesamanskaya, A.R., Poznyakovski, A.I., Paushkin, S.V., Nierras, C.R., Cox, B.S., Ter-Avanesyan, M.D., and Tuite, M.F. (1995). The products of the SUP45 (eRF1) and SUP35 genes interact to mediate translation termination in Saccharomyces cerevisiae. EMBO J. *14*, 4365–4373.

Stott, K., Blackburn, J., Butler, P., and Perutz, M. (1995). Incorporation of glutamine repeats makes protein oligomerize: implications for neurodegenerative diseases. Proc. Natl. Acad. Sci. USA *92*, 6509–6513.

Sunde, M., and Blake, C. (1997). The structure of amyloid fibrils by electron microscopy and X-ray diffraction. Adv. Protein Chem. *50*, 123–159.

Sunde, M., Serpell, L.C., Bartlam, M., Fraser, P.E., Pepys, M.B., and Blake, C.C.F. (1997). Common core structure of amyloid fibrils by synchrotron X-ray diffraction. J. Mol. Biol. *273*, 729–739.

Ter-Avanesyan, M., Kushnirov, V., Dagkesamanskaya, A., Didichenko, S., Chernoff, Y., Inge-Vechtomov, S., and Smirnov, V. (1993).

Deletion analysis of the SUP35 gene of the yeast Saccharomyces cerevisiae reveals two non-overlapping functional regions in the encoded protein. Mol. Microbiol. *7*, 683–692.

Wetzel, R. (1997). Domain stability in immunoglobulin light chain deposition disorders. Adv. Protein Chem. *50*, 183–242.

Wickner, R.B. (1994). [URE3] as an altered URE2 protein: evidence for a prion analog in Saccharomyces cerevisiae. Science *264*, 566–569.

Wickner, R.B., Masison, D.C., and Edskes, H.K. (1995). [PSI] and [URE3] as yeast prions. Yeast *11*, 1671–1685.